

Ion-beam Assisted Sputtering of Titanium Nitride Thin Films

Timothy Draher^{1,2}, Tomas Polakovic³, Juliang Li⁴, Yi Li¹, Ulrich Welp¹, Jidong Samuel Jiang¹, John Pearson¹, Whitney Armstrong³, Zein-Eddine Meziani³, Clarence Chang⁴, Wai-Kwong Kwok¹, Zhili Xiao^{1,2}, and Valentine Novosad^{1,*}

¹Argonne National Laboratory, Materials Science Division, Lemont Illinois, 60439, USA

²Northern Illinois University, Department of Physics, Dekalb Illinois, 60115, USA

³Argonne National Laboratory, Physics Division, Lemont Illinois, 60439, USA

⁴Argonne National Laboratory, High Energy Physics Division, Lemont Illinois, 60439, USA

*novosad@anl.gov

ABSTRACT

Titanium nitride is a material of interest for many superconducting devices such as nanowire microwave resonators and photon detectors. Thus, controlling the growth of TiN thin films with desirable properties is of high importance. This work aims to explore effects in ion beam-assisted sputtering (IBAS), where an observed increase in nominal critical temperature and upper critical fields are in tandem with previous work on Niobium nitride (NbN). We grow thin films of titanium nitride by both, the conventional method of DC reactive magnetron sputtering and the IBAS method, to compare their superconducting critical temperatures T_c as functions of thickness, sheet resistance, and nitrogen flow rate. We perform electrical and structural characterizations by electric transport and x-ray diffraction measurements. Compared to the conventional method of reactive sputtering, the IBAS technique has demonstrated a 10% increase in nominal critical temperature without noticeable variation in the lattice structure. Additionally, we explore the behavior of superconducting T_c in ultra-thin films. Trends in films grown at high nitrogen concentrations follow predictions of mean-field theory in disordered films and show suppression of superconducting T_c due to geometric effects, while nitride films grown at low nitrogen concentrations strongly deviate from the theoretical models.

Introduction

TiN has been extensively studied for its many useful mechanical, electrical, and optical properties. When fabricated into superconducting devices such as nanowire microwave resonators and photon detectors, TiN serves as an important material for fundamental structures in quantum electrical circuits, such as resonators used to multiplex large arrays of qubits¹. TiN has been shown to meet the criteria desired for quantum computations and photon detection such as low RF losses at both high and low driving powers, high kinetic inductance, and tunable T_c ¹⁻⁸. In addition, as a superconducting nitride, TiN has a high superconducting T_c , relative to elemental Ti and Ti₂N, for highly stoichiometric phases. It is a hard, mechanically robust, and stable material⁹⁻¹². The composition of deposited TiN_x compounds can be varied by changing the flux of reactive nitrogen gas present during fabrication, where varying the nitrogen concentration not only tunes the superconducting T_c , but also alters the film's crystal structure and kinetic inductance^{12,13}.

For the lowest nitrogen concentrations, an α -Ti phase initially forms where nitrogen is incorporated interstitially. With little increase in nitrogen, there is an atomic fraction of nitrogen that forms the Ti₂N phase which is known to suppress T_c in Ti-N compounds¹⁴. Next, in the higher nitrogen flow regime, TiN becomes the most predominant and stable compound¹⁵. A mix of the TiN (111) and TiN (002) phases can form. TiN (002) is the orientation with lower surface energy and forms more elastic grains comparatively to TiN (111), however, many deposition parameters can drive the preferred growth of either orientation such as the deposition pressure, substrate bias/temperature, ion flux, and gas composition^{14,16,17}. Growth of TiN can be conducted using a variety of physical vapor deposition (PVD) techniques including sputtering, evaporation, and molecular beam epitaxy (MBE).

MBE allows for highly stoichiometric and ordered growth of multi-component films like TiN at low temperatures inside an ultra-high vacuum environment¹⁸, while the use of reactive sputtering or evaporation promotes a more polycrystalline and amorphous lattice structure. The latter techniques offer faster growth and higher throughput at the cost of less control over crystal structure during deposition. However, sputtering and evaporation still offers the ability to grow films of high quality with desirable characteristics by tailoring the deposition parameters⁹.

In reactive DC magnetron sputtering, the target material is connected to a high power DC source that creates a plasma out of a mixture of inert gas (usually argon) and a reactive gas (in this case nitrogen) which is then confined by magnetic fields

local to the source target. The gas particles are ionized by the strong electric fields and are accelerated towards the target, which knocks loose the desired sputtering atoms that then recombine with the reactive gas to form the thin film. Ion-beam assisted sputtering (IBAS) utilizes the enhanced kinematic effects of an additional ion source to bombard the sample surface during the reactive sputtering process. This effectively anneals the film surface, and promotes better adhesion^{19,20}. In the case of reactive IBAS, the ion-beam source also functions as the supply of the reactive gas.

In a previous work with niobium nitride, IBAS was shown to decrease the sensitivity of nitrogen to forming ideal superconducting stoichiometric films and increase T_c ²¹. In this study, we aim to compare the IBAS method with conventional reactive magnetron sputtering of TiN and explore its effects on superconducting T_c , structure, and electrical properties.

Methods

TiN films were deposited on 2-inch high resistance ($\rho > 10 \text{ k}\Omega\text{cm}$) Si (100) wafers with a thin layer of native oxide inside a commercial ultra-high vacuum sputtering system from Angstrom Engineering²². Two separate growth techniques were utilized at room temperature. The first being conventional DC reactive magnetron sputtering and the second with the added bombardment of nitrogen ions from a diffusive ion-beam source, adapting the IBAS method. Before deposition, the chamber vacuum was pumped down to 5×10^{-9} Torr and the substrate surface was etched of water or organic contamination using a low energy argon ion beam. Moreover, the substrate was continuously rotated during deposition to assure uniform film growth. Samples were not heated or annealed during deposition and the temperature did not exceed 30 °C. Sputtering rates were determined by use of x-ray reflectometry and profilometer measurements on a masked twin sample.

For both methods, the chamber pressure was held fixed at 3 mTorr with a continuous mass flow of 99.9999% argon at 30 sccm. While the reactive ultrahigh purity (99.9997%) nitrogen gas concentration was varied from 0 up to 10 sccm. A 99.995% titanium target was sputtered from a 3-inch diameter magnetron sputtering gun powered by a DC power source with $P \approx 11.6 \text{ W}\cdot\text{cm}^{-2}$. The substrate-to-target distance sits at 5-inches with a 33° angle relative to the substrate surface normal. The ion-beam source was an end-Hall ion gun with attached hollow cathode for thermionic emission of electrons to neutralize the beam plasma²³. It rests at a 40° angle from the substrate and 20° azimuthal from the Ti gun. During IBAS deposition, the nitrogen flow is supplied only from the ion source rather than uniformly around the substrate during conventional sputtering. Ion energies of N_2 were kept low at 100 eV to minimize any structural damage to the films and reducing the formation of microcracks that lead to pores along the surface^{24,25}. While maintaining a 0.5 A ion current, this is equivalent to an ion power density of $70 \text{ mW}\cdot\text{cm}^{-2}$. Table 1 summarizes the general deposition parameters used.

The superconducting T_c of the TiN films was measured via a standard four-wire probe method in an ICEoxford Dry Ice cryostat and Bluefors dilution refrigerator. In addition, x-ray diffraction (XRD) analysis was conducted on films grown from both methods to determine the phase of TiN. Sheet resistance measurements followed via a four probe on a circular sample, to correct for geometric factors²⁶.

Parameter	Value
Base Pressure (Torr)	5×10^{-9}
Working Pressure (mTorr)	3
Nitrogen Flow (sccm)	0 - 10
Argon Flow (sccm)	30
Target/Substrate Distance (inch)	5
Deposition Temperature (°C)	≤ 30
Ion Energy (eV)	100
Ion Current (A)	0.5

Table 1. TiN sputtering chamber deposition parameters.

Results

The advantages of the IBAS method for TiN are best demonstrated by direct comparison of superconducting critical temperatures of thin films grown by conventional reactive sputtering under identical chemical conditions as the IBAS films.

The nitrogen flow dependence on superconducting T_c for 300 nm films grown with both techniques is shown by Fig. 1 with resistive transitions inset for IBAS grown films. While the superconducting T_c changes little with higher nitrogen flow rates, there is large variation near the flow range of 0.5-2 sccm, where the T_c increases sharply from 0.5 K to 4-4.5 K. The IBAS grown films show a 10% increase in nominal superconducting T_c . The sharp increase in the superconducting T_c is due to the formation of stoichiometric TiN as the nitrogen content increases¹².

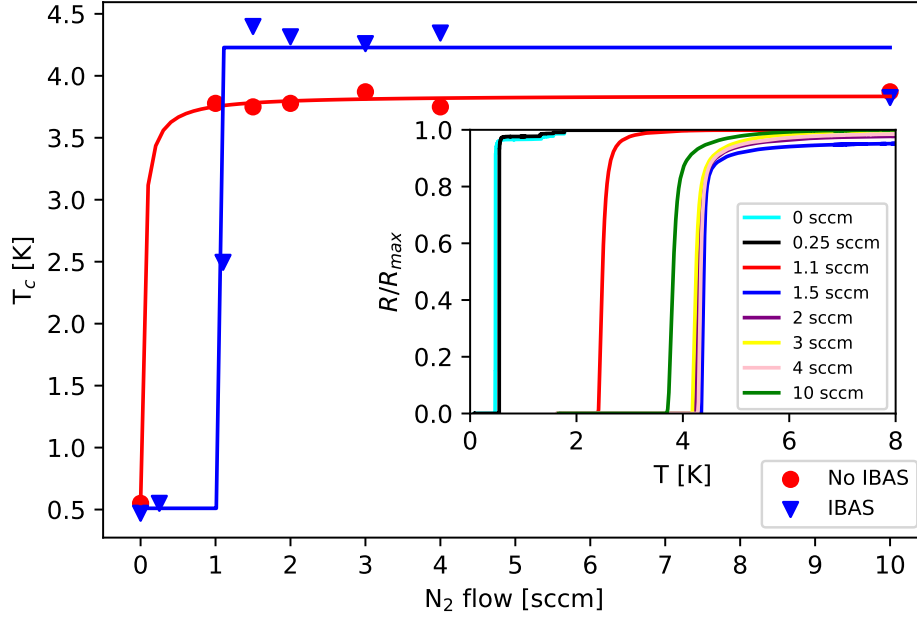


Figure 1. Comparison of bulk 300nm TiN films dependence of T_c on nitrogen flow rates under reactive magnetron sputtering with no ion beam assist (red) and including the ion beam (blue). Trend curves are sigmoid fits meant to serve as guides to the eye. Inset: Normalized resistance transition curves for IBAS grown films at various nitrogen flow points.

Fig. 2 shows comparative XRD $\omega - 2\theta$ scans of films grown using both methods. Beyond the transition where T_c saturates in Fig. 1, TiN (111) is the predominant and stable phase we observe in this study^{9,12}. Though it has been shown that IBAS does promote growth orientations at different ion energy and current regimes, our ion beam characteristics (100 eV ion energy and 0.5 A current) do not sufficiently promote any predominant orientation outside of TiN (111)^{19,27,28}. The sputtering gas composition of argon and nitrogen used (100 - 75% Ar and 0 - 25% N₂) is also attributed to the preferential growth of TiN (111)¹⁷. Argon's presence during sputtering promotes a more metallic growth mode rather than nitridic. In the metallic growth mode, Ti adatoms react with nitrogen on the substrate surface²⁹. However, before reacting, the Ti adatoms collect together in clusters and form low surface energy (111) planes. (111) stacks alternating layers of Ti and interstitial N resulting in rapid columnar grain growth normal to the substrate surface. The (002) orientation has the lowest surface energy and therefore the adatoms ability to diffuse outward is easier but a far slower process comparatively. Thus, the faster (111) orientation is preferred and is a factor of the limited kinetics provided by the ion source and Ar-N₂ gas composition.

The upper critical magnetic field H_{c2} and coherence length ξ of the nominal 4 sccm IBAS film was determined by measurements of various fields perpendicular to the sample surface near T_c . From these values, the $H_{c2}(T = 0)$ can be calculated by the Werthamer-Helfand-Hohenberg formula³⁰.

$$H_{c2}(0) = -0.69T_c \left. \frac{dH_{c2}}{dT} \right|_{T_c}. \quad (1)$$

Then the in-plane Ginzburg-Landau coherence length can be calculated via,

$$H_{c2}(T) = \frac{\Phi_0}{2\pi\xi^2(T)}, \quad (2)$$

where Φ_0 is the single flux quantum³¹. Nominally this method is well founded in the region close to T_c , but in practice, it can be applied deeply into the superconducting state. Upper critical field measurement for a nominal IBAS film (300 nm at 4 sccm) can be seen in Fig. 3. The calculated perpendicular critical field was found to be $H_{c2}(0) = 85.4$ kOe with estimated coherence length of $\xi(0) = 1.96$ nm from fitting. The low value of $\xi(0)$ is suspected to be caused by disorder in the sputtered films, where

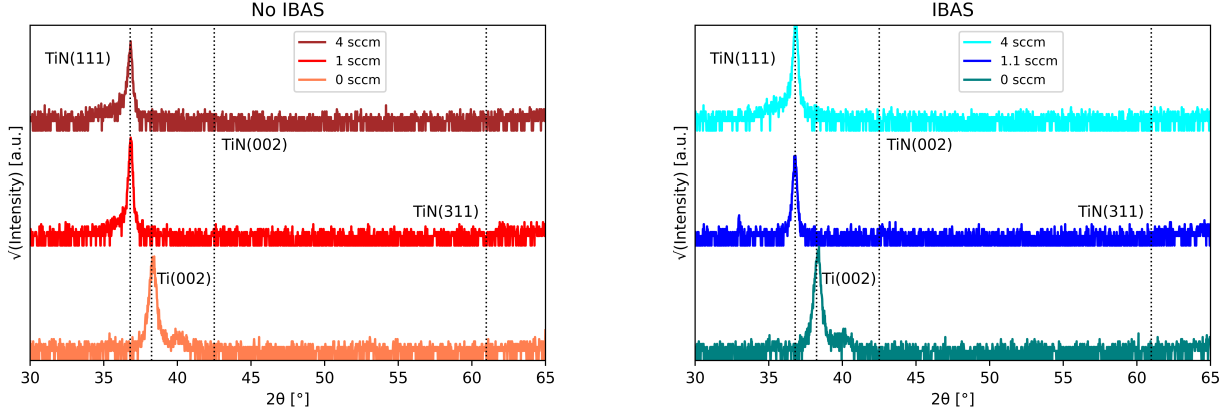


Figure 2. XRD $\omega - 2\theta$ scans of 300 nm TiN films grown at room temperature via conventional reactive magnetron sputtering (left) and IBAS growth method (right) at varying nitrogen flow rates. TiN (111) is the primary orientation selected and Ti (002) is grown with no nitrogen added during deposition.

the renormalization due to short electronic mean free path l is approximately $\xi^* = 0.85\sqrt{\xi \times l^{32}}$. If we assume unperturbed $\xi = 105 \text{ nm}^{33}$, we end up with mean free path of approximately 4 \AA , which is within the reported range $[3.5-7.3] \text{ \AA}$ for TiN³⁴.

Many applications of superconducting devices often require the material to be in the form of a thin film. Because of that, we also study the dependence of superconducting T_c and its resistance on film thickness. There are many models for suppression of the superconducting state with decreasing film thickness. In this class of materials, the demise of superconducting state is often explained by either weak localization effects or electron wave leakage^{35–37}.

The electron leakage model describes the suppression a geometric effect where the electron wave function treated as a infinite well state in the direction perpendicular to the sample surface. To preserve charge balance across the thin films, one has to nominally allow for this well to extend beyond the geometric boundary of the film, with a characteristic length as a parameter of the model. This reduces the cooper pair density of states and suppresses T_c . This model's expression for the behavior of $T_c(d)$ can be shown as³⁶

$$T_c = T_{c\infty} \exp\left[\frac{-b}{N(0)Vd}\right] \quad (3)$$

where $T_{c\infty}$ is the superconducting critical temperature of a bulk sample, b is the characteristic length of electron wave leakage, and $N(0)V$ is the BCS coupling constant. By using known values for the Debye temperature θ_D (for TiN of 746-769 K³⁸), and the superconducting energy gap Δ of 3 meV, we can extract the BCS coupling of $N(0)V = 0.165$ and use it to determine the leakage parameters in our films. Considering the disordered nature of sputtered films, one can further modify Eq. (3) to account for the presence of defects and film breakup with,

$$T_c = T_{c\infty} \exp\left[\frac{-1}{N(0)V} \left(\frac{b}{d} + \frac{c}{d^2}\right)\right] \quad (4)$$

where c is the parameter that accounts for film breakup and defects. Fig. 4 demonstrates the dependence of superconducting T_c on film thickness d for both deposition methods at nitrogen flow points of 1 sccm for the non-IBAS films, and 1.1 sccm and 4 sccm for IBAS, respectively. With application of the simpler model, we extract $b = 4.58 \text{ \AA}$ for the 1 sccm non-IBAS films, and $b = 2.30 \text{ \AA}$ for the 4 sccm IBAS films. Turning to Eq. (4), a quantitatively better fit for 1 sccm non-IBAS yields values of $b = 5.97 \times 10^{-7} \text{ \AA}$ and $c = 139.6 \text{ \AA}^2$, however, these values are outside of reasonable ranges (where b should be on the order of electron Fermi wavelength). For 4 sccm IBAS films, the corrected model also fails with $b = 3.72 \text{ \AA}$ and the nonphysical value of $c = -43.6 \text{ \AA}^2$. Considering the almost linear trend of $\log(T_c)$ for the 4 sccm films in Fig. 4, it is justifiable to use the simple electron leakage theory as a valid model. The 1.1 sccm IBAS films heavily deviate from the leakage models and the suppression of superconducting T_c has to be driven by a different mechanism.

Another approach to explore the suppression of superconducting T_c is by observing the films sheet resistance on T_c . Ivry *et*

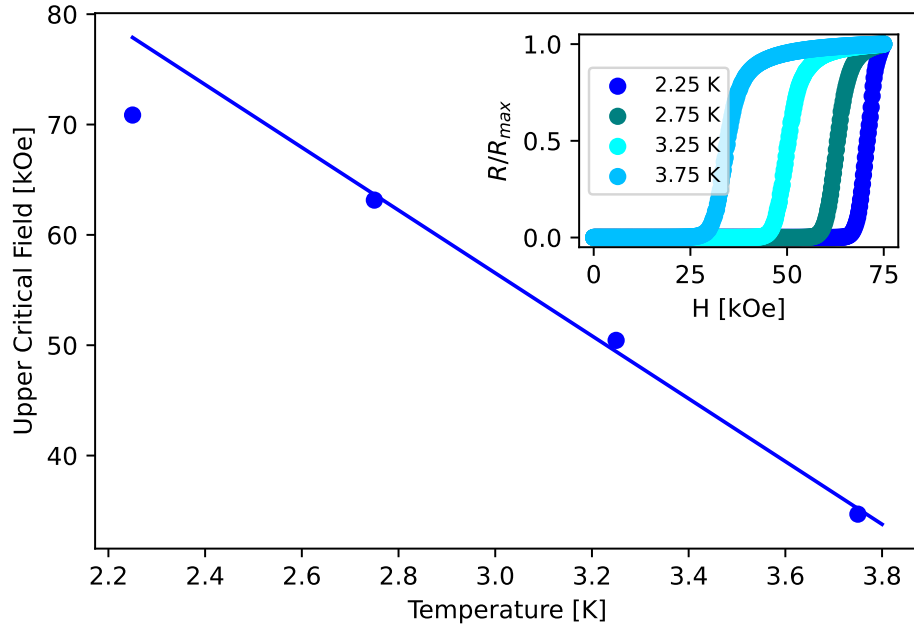


Figure 3. Perpendicular upper critical field H_{c2} measured as a function of temperature for a 300 nm IBAS thin film deposited at 4 sccm. Inset: Normalized resistance measurements of the same film as a function of the applied field at temperatures close to T_c .

al. propose an universal phenomenological power-law relationship

$$d \cdot T_c = AR_{sheet}^{-B} \quad (5)$$

where R_{sheet} is the sheet resistance and A and B are fitting parameters³⁹, with B related to the BCS coupling $N(0)V$ in the weak coupling limit⁴⁰. Fig. 5 shows the scaled T_c as a function of R_{sheet} . Where the 1 sccm non-IBAS films follow the Ivry fit with $B = 0.58$. The IBAS films show different behavior with decreasing nitrogen flow. The 4 sccm films still follow the power-law with $B = 0.24$ while the 1.1 sccm films again deviates largely. The B values of both sets of films are lower than for films grown by atomic layer deposition gathered and reported by Ivry $B \approx [0.81 - 0.96]$ but within the general range of the phenomenological theory.

A more first-principles approach is to employ results of renormalization methods to further attempt to explain the suppression of T_c ⁴¹:

$$\frac{T_c}{T_{c\infty}} = \exp\left[\frac{-1}{\gamma}\right] \times \left[\frac{1 + \frac{\sqrt{r/2}}{\gamma - r/4}}{1 - \frac{\sqrt{r/2}}{\gamma - r/4}}\right]^{1/\sqrt{2r}} \quad (6)$$

where $\gamma = \frac{1}{\log(k_b T_{c\infty} \tau / \hbar)}$ and $r = \frac{R_{sheet}}{(2\pi^2 \hbar / e^2)}$, k_b is the Boltzmann constant, e is the elementary charge, and τ is the electron elastic scattering time. Fig. 6 shows the approximately linear behavior of the 1 sccm non-IBAS films with $\tau = 1.59 \times 10^{-15}$ s and similarly $\tau = 1.63 \times 10^{-15}$ s for the 4 sccm IBAS set. Notably, the 1.1 sccm IBAS films again stray away from the model. This further suggests that within the nitrogen flow transition region, where T_c rises rapidly (Fig. 1), the IBAS process has a substantial effect on the mesoscale structure of the films.

A potential mechanism driving the suppression of T_c and increase of resistivity is due to lattice point defects such as oxygen substitutions and nitrogen vacancies, which are possible in the nitrogen-poor environment at low N_2 flows⁴². The ion beam increases adatom mobility by imparting increased momentum of incident nitrogen ions onto the substrate, which increases the probability that such defects could occur, especially around this critical nitrogen flow point, where formation of stoichiometric

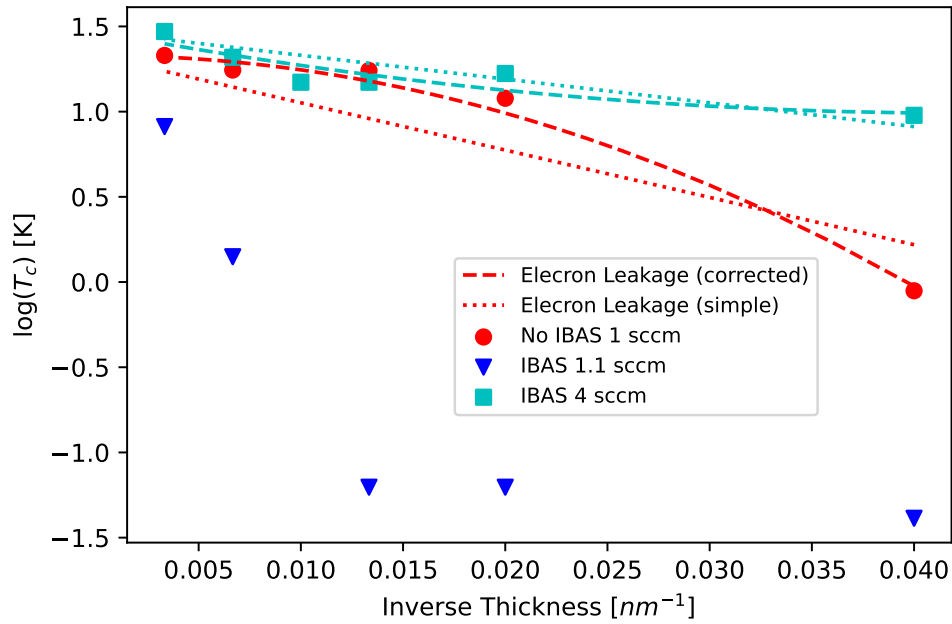


Figure 4. Dependence of superconducting T_c on inverse film thickness consisting of different nitrogen flows. Experimental data are plotted in red circles (non-IBAS) contrasted with blue triangles and cyan squares (IBAS). Lines show best fits of different models: The dotted lines are a fit of Eq. (3) and the dashed lines corresponds to a fit of Eq. (4). The 1.1 scc IBAS films do not follow either model.

TiN begins to form. In addition, we conducted atomic force microscopy imaging that revealed little difference in morphologies between the 1 and 4 sccm samples for both growth methods. The only difference we could identify is that the grain sizes were larger for the 4 sccm samples, as expected¹⁷.

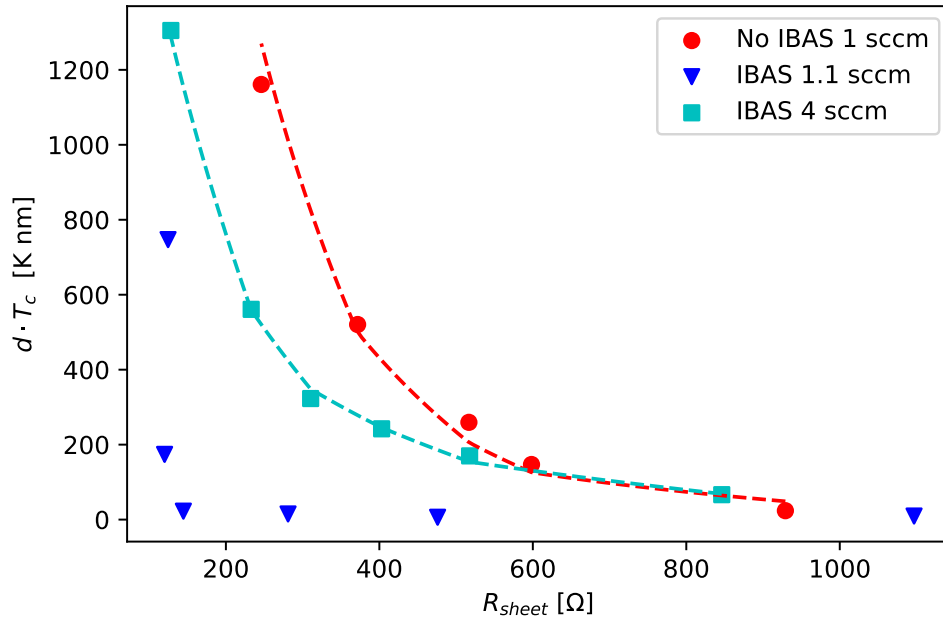


Figure 5. Dependence of superconducting T_c scaled by thickness on sheet resistance for different nitrogen flows. Experimental data for 1 sccm non-IBAS films (red) and 1.1 (blue) and 4 sccm (cyan) IBAS films are shown respectively. The dashed lines are fits of Eq. (5) while the 1.1 sccm IBAS films heavily deviate from the model.

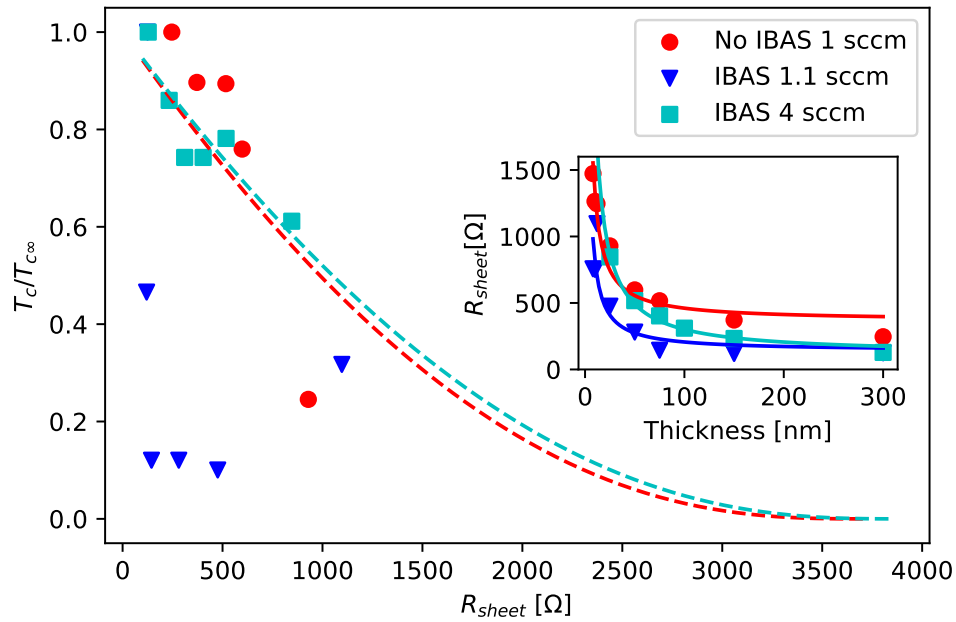


Figure 6. Dependence of superconducting T_c on sheet resistance. The 1 sccm non-IBAS (red), 1.1 sccm (blue) and 4 sccm (cyan) IBAS films are shown. The red and cyan curves are experimental fits of the data to Eq. (6). The blue 1 sccm IBAS data does not follow the same model. Inset: dependence of sheet resistance on film thickness where all three curves follow a similar $\frac{1}{d}$ dependence.

Discussion

In this study, we have investigated the superconducting properties of TiN thin films grown by two different methods: DC reactive sputtering and ion-beam assisted sputtering (IBAS) at room temperature. Our results have shown that the IBAS method has several benefits when compared to the DC reactive sputtering method. Specifically, we have observed a 10% higher nominal critical temperature using the IBAS method.

The behavior of the superconducting critical temperature T_c in films grown at high nitrogen concentrations follows the predictions of the electron leakage model and mean-field theory for disordered thin films. These models suggest that a higher nitrogen concentration promotes a more uniform film with fewer non-superconducting interfacial layers, leading to an increase in T_c . However, in the lower nitrogen flow regime, the experimental data deviates heavily from these models. We observed a non-monotonous trend in T_c as a function of thickness and resistivity, which is an effect that requires further exploration and deserves a separate future study.

Data Availability

The datasets generated during and/or analysed during the current study are available from the corresponding author on reasonable request.

References

1. Baselmans, J. J. A. *et al.* Development of high-q superconducting resonators for use as kinetic inductance detectors. *Adv. Space Res.* **40**, 708–713, DOI: <https://doi.org/10.1016/j.asr.2007.06.041> (2007).
2. Wallraff, A. *et al.* Strong coupling of a single photon to a superconducting qubit using circuit quantum electrodynamics. *Nature* **431**, 162–167 (2004).
3. Vissers, M. R. *et al.* Low loss superconducting titanium nitride coplanar waveguide resonators. *Appl. Phys. Lett.* **97**, 232509, DOI: [10.1063/1.3517252](https://doi.org/10.1063/1.3517252) (2010).
4. Gao, J. *et al.* Experimental evidence for a surface distribution of two-level systems in superconducting lithographed microwave resonators. *Appl. Phys. Lett.* **92**, 152505, DOI: [10.1063/1.2906373](https://doi.org/10.1063/1.2906373) (2008).
5. Sandberg, M. *et al.* Etch induced microwave losses in titanium nitride superconducting resonators. *Appl. Phys. Lett.* **100**, 262605, DOI: [10.1063/1.4729623](https://doi.org/10.1063/1.4729623) (2012).
6. Leduc, H. *et al.* Titanium nitride films for ultrasensitive microresonator detectors. *Appl. Phys. Lett.* **97**, DOI: [10.1063/1.3480420](https://doi.org/10.1063/1.3480420) (2010).
7. Mazin, B. A. *et al.* Position sensitive x-ray spectrophotometer using microwave kinetic inductance detectors. *Appl. Phys. Lett.* **89**, 222507, DOI: [10.1063/1.2390664](https://doi.org/10.1063/1.2390664) (2006).
8. Bretz-Sullivan, T. M. *et al.* High kinetic inductance nbtin superconducting transmission line resonators in the very thin film limit. *Appl. Phys. Lett.* **121**, 52602, DOI: [10.1063/5.0100961](https://doi.org/10.1063/5.0100961) (2022).
9. Jeyachandran, Y. L., Narayandass, S., Mangalaraj, D., Areva, S. & Mielczarski, J. A. Properties of titanium nitride films prepared by direct current magnetron sputtering. *Mater. Sci. Eng. A* **445-446**, 223–236, DOI: <https://doi.org/10.1016/j.msea.2006.09.021> (2007).
10. Diserens, M., Patscheider, J. & Lévy, F. Improving the properties of titanium nitride by incorporation of silicon. *Surf. Coatings Technol.* **108-109**, 241–246, DOI: [https://doi.org/10.1016/S0257-8972\(98\)00560-X](https://doi.org/10.1016/S0257-8972(98)00560-X) (1998).
11. Wu, H. Z. *et al.* Characterization of titanium nitride thin films. *Thin Solid Films* **191**, 55–67, DOI: [https://doi.org/10.1016/0040-6090\(90\)90274-H](https://doi.org/10.1016/0040-6090(90)90274-H) (1990).
12. Vissers, M. R. *et al.* Characterization and in-situ monitoring of sub-stoichiometric adjustable superconducting critical temperature titanium nitride growth. *Thin Solid Films* **548**, 485–488, DOI: <https://doi.org/10.1016/j.tsf.2013.07.046> (2013).
13. Adjaottor, A., Meletis, E., Logothetidis, S., Alexandrou, I. & Kokkou, S. Effect of substrate bias on sputter-deposited tixx, tiny and tixny thin films. *Surf. Coatings Technol.* **76-77**, 142–148, DOI: [10.1016/0257-8972\(95\)02594-4](https://doi.org/10.1016/0257-8972(95)02594-4) (1995).
14. Greene, J. E., Sundgren, J., Hultman, L., Petrov, I. & Bergstrom, D. B. Development of preferred orientation in polycrystalline tin layers grown by ultrahigh vacuum reactive magnetron sputtering. *Appl. Phys. Lett.* **67**, 2928–2930, DOI: [10.1063/1.114845](https://doi.org/10.1063/1.114845) (1995).
15. Spengler, W., Kaiser, R., Christensen, A. N. & Müller-Vogt, G. Raman scattering, superconductivity, and phonon density of states of stoichiometric and nonstoichiometric tin. *Phys. Rev. B* **17**, 1095–1101, DOI: [10.1103/PhysRevB.17.1095](https://doi.org/10.1103/PhysRevB.17.1095) (1978).

16. Patsalas, P., Charitidis, C. & Logothetidis, S. The effect of substrate temperature and biasing on the mechanical properties and structure of sputtered titanium nitride thin films. *Surf. Coatings Technol.* **125**, 335–340, DOI: [10.1016/S0257-8972\(99\)00606-4](https://doi.org/10.1016/S0257-8972(99)00606-4) (2000).
17. Banerjee, R., Chandra, R. & Ayyub, P. Influence of the sputtering gas on the preferred orientation of nanocrystalline titanium nitride thin films. *Thin Solid Films* **405**, 64–72, DOI: [10.1016/S0040-6090\(01\)01705-9](https://doi.org/10.1016/S0040-6090(01)01705-9) (2002).
18. Rasic, D., Sachan, R., Chisholm, M. F., Prater, J. & Narayan, J. Room temperature growth of epitaxial titanium nitride films by pulsed laser deposition. *Cryst. Growth & Des.* **17**, 6634–6640, DOI: [10.1021/acs.cgd.7b01278](https://doi.org/10.1021/acs.cgd.7b01278) (2017). Doi: [10.1021/acs.cgd.7b01278](https://doi.org/10.1021/acs.cgd.7b01278).
19. Zhang, L., Tong, S., Liu, H., Li, Y. & Wang, Z. Effects of sputtering and assisting ions on the orientation of titanium nitride films fabricated by ion beam assisted sputtering deposition from metal target. *Mater. Lett.* **171**, 304–307, DOI: <https://doi.org/10.1016/j.matlet.2016.02.100> (2016).
20. Hirsch, E. & Varga, I. Thin film annealing by ion bombardment. *Thin Solid Films* **69**, 99–105, DOI: [10.1016/0040-6090\(80\)90207-2](https://doi.org/10.1016/0040-6090(80)90207-2) (1980).
21. Polakovic, T. *et al.* Room temperature deposition of superconducting niobium nitride films by ion beam assisted sputtering. *APL Mater.* **6**, 76107, DOI: [10.1063/1.5031904](https://doi.org/10.1063/1.5031904) (2018).
22. See <https://angstromengineering.com/products/evovac/> for details corresponding to the sputtering system.
23. Kaufman, H. R., Robinson, R. S. & Seddon, R. I. End-hall ion source. *J. Vac. Sci. & Technol. A: Vacuum, Surfaces, Films* **5**, 2081–2084, DOI: [10.1116/1.574924](https://doi.org/10.1116/1.574924) (1987).
24. Marchenko, I. G. & Neklyudov, I. M. Film nanostructure formation during low-temperature pvd deposition using partially ionized atomic fluxes. *J. Physics: Conf. Ser.* **113**, 012014, DOI: [10.1088/1742-6596/113/1/012014](https://doi.org/10.1088/1742-6596/113/1/012014) (2008).
25. Hibbs, M., Johansson, B., Sundgren, J.-E. & Helmersson, U. Effects of substrate temperature and substrate material on the structure of reactively sputtered tin films. *Thin Solid Films* **122**, 115–129, DOI: [10.1016/0040-6090\(84\)90003-8](https://doi.org/10.1016/0040-6090(84)90003-8) (1984).
26. Yilmaz, S. The geometric resistivity correction factor for several geometrical samples. *J. Semicond.* **36**, 082001 (2015).
27. Patsalas, P., Gravalidis, C. & Logothetidis, S. Surface kinetics and subplantation phenomena affecting the texture, morphology, stress, and growth evolution of titanium nitride films. *J. Appl. Phys.* **96**, 6234–6246, DOI: [10.1063/1.1811389](https://doi.org/10.1063/1.1811389) (2004).
28. Patsalas, P. & Logothetidis, S. Optical, electronic, and transport properties of nanocrystalline titanium nitride thin films. *J. Appl. Phys.* **90**, 4725–4734, DOI: [10.1063/1.1403677](https://doi.org/10.1063/1.1403677) (2001).
29. Lungu, C., Futsuhara, M., Takai, O., Braic, M. & Musa, G. Noble gas influence on reactive radio frequency magnetron sputter deposition of tin films. *Vacuum* **51**, 635–640, DOI: [10.1016/S0042-207X\(98\)00264-4](https://doi.org/10.1016/S0042-207X(98)00264-4) (1998).
30. Werthamer, N. R., Helfand, E. & Hohenberg, P. C. Temperature and purity dependence of the superconducting critical field, H_{c2} . iii. electron spin and spin-orbit effects. *Phys. Rev.* **147**, 295–302, DOI: [10.1103/PhysRev.147.295](https://doi.org/10.1103/PhysRev.147.295) (1966).
31. Tinkham, M. *Introduction to Superconductivity / Michael Tinkham* (McGraw-Hill, 1975).
32. Caroli, C., De Gennes, P. & Matricon, J. Coherence length and penetration depth of dirty superconductors. *Physik der kondensierten Materie* **1**, 176–190 (1963).
33. Faley, M. I., Liu, Y. & Dunin-Borkowski, R. E. Titanium nitride as a new prospective material for nanosquids and superconducting nanobridge electronics. *Nanomaterials* **11**, 466 (2021).
34. Kardakova, A. I. *et al.* Electron–phonon energy relaxation time in thin strongly disordered titanium nitride films. *IEEE Transactions on Appl. Supercond.* **25**, 1–4, DOI: [10.1109/TASC.2014.2364516](https://doi.org/10.1109/TASC.2014.2364516) (2015).
35. Graybeal, J. M. & Beasley, M. R. Localization and interaction effects in ultrathin amorphous superconducting films. *Phys. Rev. B* **29**, 4167–4169, DOI: [10.1103/PhysRevB.29.4167](https://doi.org/10.1103/PhysRevB.29.4167) (1984).
36. Yu, M., Strongin, M. & Paskin, A. Consistent calculation of boundary effects in thin superconducting films. *Phys. Rev. B* **14**, 996–1001, DOI: [10.1103/PhysRevB.14.996](https://doi.org/10.1103/PhysRevB.14.996) (1976).
37. Maekawa, S. & Fukuyama, H. Localization effects in two-dimensional superconductors. *J. Phys. Soc. Jpn.* **51**, 1380–1385, DOI: [10.1143/JPSJ.51.1380](https://doi.org/10.1143/JPSJ.51.1380) (1982).
38. Kozma, A. Thermodynamic, thermal and elastic properties of titanium nitride tin: Comparison of various data and determination of the most reliable values. *Technol. transfer: fundamental principles innovative technical solutions* **4**, 14–17, DOI: [10.21303/2585-6847.2020.001475](https://doi.org/10.21303/2585-6847.2020.001475) (2020).

39. Ivry, Y. *et al.* Universal scaling of the critical temperature for thin films near the superconducting-to-insulating transition. *Phys. Rev. B* **90**, 214515, DOI: [10.1103/PhysRevB.90.214515](https://doi.org/10.1103/PhysRevB.90.214515) (2014).
40. McMillan, W. L. Transition temperature of strong-coupled superconductors. *Phys. Rev.* **167**, 331–344, DOI: [10.1103/PhysRev.167.331](https://doi.org/10.1103/PhysRev.167.331) (1968).
41. Finkel'stein, A. M. Suppression of superconductivity in homogeneously disordered systems. *Phys. B: Condens. Matter* **197**, 636–648, DOI: [https://doi.org/10.1016/0921-4526\(94\)90267-4](https://doi.org/10.1016/0921-4526(94)90267-4) (1994).
42. Ohya, S. *et al.* Room temperature deposition of sputtered tin films for superconducting coplanar waveguide resonators. *Supercond. Sci. Technol.* **27**, 015009, DOI: [10.1088/0953-2048/27/1/015009](https://doi.org/10.1088/0953-2048/27/1/015009) (2014).

Acknowledgements

This work was supported by the U. S. Department of Energy (DOE), Office of Science, Offices of Nuclear Physics, Basic Energy Sciences, Materials Sciences and Engineering Division under Contract # DE-AC02-06CH11357.

Author contributions statement

Thin film growth and transport measurements conducted by T.D. Dilution refrigerator transport measurements conducted by J.L. Manuscript and analysis of results due to T.D. and T.P. All authors reviewed the manuscript.

Competing Interests

The authors declare no competing interests.

Additional information

Correspondence and requests for materials should be addressed to V.N.